

# Impact of Evapotranspiration on Dry Season Climate in the Amazon Forest\*

ANNA HARPER

*College of Engineering, Mathematics, and Physical Sciences, University of Exeter, Exeter, Devon, United Kingdom,  
and Department of Atmospheric Science, Colorado State University, Fort Collins, Colorado*

IAN T. BAKER, A. SCOTT DENNING, DAVID A. RANDALL, DONALD DAZLICH, AND MARK BRANSON

*Department of Atmospheric Science, Colorado State University, Fort Collins, Colorado*

(Manuscript received 30 January 2013, in final form 30 August 2013)

## ABSTRACT

Moisture recycling can be an important source of rainfall over the Amazon forest, but this process relies heavily upon the ability of plants to access soil moisture. Evapotranspiration (ET) in the Amazon is often maintained or even enhanced during the dry season, when net radiation is high. However, ecosystem models often over predict the dry season water stress. The authors removed unrealistic water stress in an ecosystem model [the Simple Biosphere Model, version 3 (SiB3)] and examined the impacts of enhanced ET on the dry season climate when coupled to a GCM. The “stressed” model experiences dry season water stress and limitations on ET, while the “unstressed” model has enhanced root water access and exhibits strong drought tolerance.

During the dry season in the southeastern Amazon, SiB3 unstressed has significantly higher latent heat flux (LH) and lower sensible heat flux (SH) than SiB3 stressed. There are two competing impacts on the climate in SiB3 unstressed: cooling resulting from lower SH and moistening resulting from higher LH. During the average dry season, the cooling plays a larger role and the atmosphere is more statically stable, resulting in less precipitation than in SiB3 stressed. During dry season droughts, significantly higher LH in SiB3 unstressed is a necessary but not sufficient condition for stronger precipitation. The moistening effect of LH dominates when the Bowen ratio ( $BR = SH/LH$ ) is  $>1.0$  in SiB3 stressed and precipitation is up to 26% higher in SiB3 unstressed. An implication of this analysis is that forest conservation could enable the Amazon to cope with drying conditions in the future.

## 1. Introduction

The Amazon forest stores huge amounts of carbon in its biomass (Saatchi et al. 2007, 2011), but its future is uncertain because of the combined threats of climate change and deforestation (Nepstad et al. 2008; Malhi et al. 2008). Recent Amazonian droughts have led to decreases in biomass (Phillips et al. 2009; Lewis et al. 2011; Toomey et al. 2011) and increases in tree mortality (Phillips et al.

2010), and several GCMs predict reduced dry season precipitation throughout the twenty-first century (Malhi et al. 2008). Amazon droughts are linked to variability in the tropical Atlantic and Pacific sea surface temperatures (Liebmann and Marengo 2001; Marengo 2004; Chen et al. 2011). An anomalously warm tropical North Atlantic displaces the intertropical convergence zone (ITCZ) northward (Marengo et al. 2011), which weakens the trade winds, reduces water vapor transport, and increases subsidence above the central and southern Amazon (Espinoza et al. 2011). In effect, these meteorological changes lengthen the dry season, and data from the Global Precipitation Climatology Centre suggest that dry seasons have become longer since the 1990s (Marengo et al. 2011). El Niño events are associated with drought in the northeastern Amazon (Ropelewski and Halpert 1987; Chen et al. 2011) and large-scale subsidence due to a shift in the Walker circulation (Malhi and Wright 2004). Two recent

---

\* Supplemental information related to this paper is available at the Journals Online website: <http://dx.doi.org/10.1175/JCLI-D-13-00074.s1>.

---

*Corresponding author address:* Anna Harper, Laver Building, North Park Road, University of Exeter, Exeter, Devon EX4 4QE, United Kingdom.  
E-mail: [a.harper@exeter.ac.uk](mailto:a.harper@exeter.ac.uk)

severe droughts (in 2005 and 2010) attracted attention because of their severity and ecological impacts. Both droughts were linked to an anomalously warm tropical North Atlantic (Marengo et al. 2008b; Espinoza et al. 2011), a pattern that is predicted to continue or perhaps increase (Cox et al. 2008). In 2005, drought coincided with the dry season and resulted in significant biomass reductions (Aragao et al. 2008; Zeng et al. 2008; Phillips et al. 2009) related to both heat and moisture stress (Toomey et al. 2011). The severe drought in 2010 affected a larger area, negatively impacted biomass (Lewis et al. 2011), and resulted in widespread declines in vegetation greenness (Xu et al. 2011). This drought was preceded by an El Niño, which limited wet season precipitation and contributed to the severity of the drought (Marengo et al. 2011).

During a drought, plants may close their stomata to limit water loss (Fisher et al. 2006), which can lead to mortality as the plants cease to assimilate carbon. Whether plant stomata remain open or closed during a drought also impacts the latent heat flux (LH) between the land and atmosphere. On average, moisture recycling due to evaporation from the land surface contributes between one-quarter and one-third of the precipitation over the Amazon, although this number varies in space and time (Eltahir and Bras 1994; Trenberth 1999). Evapotranspiration (ET) serves as a significant source of precipitation (Spracklen et al. 2012), and loss of forest cover has been linked to drying in the southern Amazon over the past 30 years (Lee et al. 2011). Moisture recycling can impact dry season climate by affecting the timing of the wet season onset (Fu and Li 2004; Li and Fu 2004). Prior to the transition from dry to wet season, surface LH increases the atmosphere's convective available potential energy (CAPE) and decreases convective inhibition energy (CINE). These processes increase rainfall and initiate the transition period (Fu and Li 2004). When the land surface is anomalously dry, LH is lower and sensible heat (SH) is higher than average. CINE remains high and the wet season onset is delayed (Fu and Li 2004).

If stomatal conductance is severely limited during a drought, reduced ET could reduce moisture recycling and reinforce drought conditions. This is a positive feedback on drought, analogous to the delayed wet season onset described by Fu and Li (2004). Conversely, plants can maintain or even increase transpiration during the dry season (Nepstad et al. 1994; Oliveira et al. 2005; Lee et al. 2005; Hasler and Avissar 2007; da Rocha et al. 2009; Costa et al. 2010). Because of the presence of deep roots and ample soil moisture, ET in the equatorial Amazon is tightly coupled to net radiation, which is higher during the dry season (Hasler and Avissar 2007).

Moving south, the seasonality of precipitation increases, as does the potential for water stress during the dry season. As a result, ET can be higher in the dry season (Costa et al. 2010; Vourlitis et al. 2011) or the wet season (Costa et al. 2010; da Rocha et al. 2009; Lathuilliere et al. 2012), depending on several factors such as vegetation type, dry season intensity, and depth to the water table. For example, in the southern Amazon, surface resistance can be twice as high during the dry season compared to the wet season (Costa et al. 2010), contributing to lower dry season ET.

It is unknown how long into a drought the trees are able to maintain predrought photosynthesis and transpiration rates, but the immediate impacts of the 2005 drought possibly included enhanced vegetation greenness (which implies increased transpiration) (Saleska et al. 2007), although a subsequent study asserted that forest "green up" did not occur (Samanta et al. 2010). Satellite-based microwave retrievals based on improved algorithms during the 2005 drought suggest a 3-month lag in the forest response to water deficits in the western Amazon, although the response was concurrent with the greatest water deficits in the northeastern Amazon (Saatchi et al. 2013). If plants continue to transpire during a drought, this could reduce the severity of the drought through moisture recycling. Evidence of this phenomenon has been observed during the wet season onset, such that when the land surface is wet, the enhanced LH can enable an earlier transition (although large-scale circulation can counteract this) (Fu and Li 2004).

Modeling studies of Amazon climate are essential for preparing for possible future climate and land cover scenarios, and it is equally important to accurately capture the impacts of ET on dry season rainfall. Models that do not allow plants to access adequate soil moisture during the dry season will overestimate the dry season Bowen ratio ( $BR = SH/LH$ ) and are more likely to induce the positive feedback cycle above. Recent developments in the Simple Biosphere Model, version 3 (SiB3), focused on accurately representing soil water stress in the Amazon. Previously, SiB predicted water limitations on photosynthesis and transpiration during the dry season. When coupled to a GCM [affectionately known as the Beautiful General Circulation Modeling System (BUGS) at Colorado State University], reduced ET severely limited precipitation above the Amazon (Randall et al. 1996). Changes to SiB3's soil and roots enabled the trees to transpire through the dry season, increased LH, reduced SH, and impacted the local climate (Baker et al. 2008; Harper et al. 2010). SiB3 can realistically simulate seasonal cycles of LH, SH, and net ecosystem exchange at a handful of sites in the Amazon

[Tapajos K83 in Baker et al. (2008); Manaus, Tapajos K67, K83, Reserva Jaru, and Pe de Gigante in Baker et al. (2013); and Tapajos K67, K83, and Caxiuana in Harper et al. (2013, manuscript submitted to *J. Geophys. Res. Biogeosci.*)].

The aim of the present study is to examine the impacts of increased ET on the dry season climate in the Amazon, using SiB3 coupled to the GCM BUGS, version 5 (BUGS5). The standard version of SiB3 represents a strongly drought resistant forest, as it includes processes documented as important for soil moisture access in the tropical forests of South America (Baker et al. 2008, 2013; Harper et al. 2013, manuscript submitted to *J. Geophys. Res. Biogeosci.*). We use a second version of SiB3 that does not include these adaptations and produces unrealistic dry season water stress. The standard version is called SiB3 unstressed (SiB3U), and the latter model is SiB3 stressed (SiB3S). We hypothesize that SiB3 stressed will produce the positive feedback addressed above (reduced dry season ET reinforcing dry conditions and further reducing precipitation). The methods of the study are outlined in section 2, and the overall performance of the BUGS5 model is discussed in section 3, with special attention on South American climate. In section 4, we assess the impacts on the dry season climate of two extreme representations of forest drought resistance.

## 2. Methods

### a. SiB3

SiB3 simulates biophysical processes and ecosystem metabolism (Sellers et al. 1986; Denning et al. 1996; Sellers et al. 1996a,b; Baker et al. 2008). Carbon assimilation accounts for enzyme kinetics (Farquhar et al. 1980) and is linked to stomatal conductance (Collatz et al. 1991, 1992). The model simulates the turbulent exchange of CO<sub>2</sub>, moisture, heat, and momentum between the free atmosphere and a prognostic canopy air space (Vidale and Stockli 2005). The surface hydrology scheme consists of water intercepted by the canopy, the ground, and a 10-layer soil model. Vertical movement of soil moisture is governed by Darcy's law, and the model has 10 soil layers that become thicker with depth. Runoff can occur as a result of subsurface drainage out of the lowest layer or resulting from excess overland flow when incoming rainfall cannot infiltrate the top layer. SiB3's ET is the sum of canopy transpiration and evaporation from puddles, the top soil layer, and the canopy. The modifications to SiB3 stressed alter the stomatal conductance; therefore, differences in the canopy transpiration dominate the model differences in ET. In the coupling with the GCM,

ET is converted to latent heat flux from the canopy air space to the mixed layer (which is the lowest GCM level).

The leaf area index (LAI) and fraction of photosynthetically active radiation (fPAR) are calculated from the normalized difference vegetation index (NDVI) from the Advanced Very High-Resolution Radiometer 4-km global area coverage data (Tucker et al. 2005). Each grid cell is assigned one biome type for the entire simulation period (Sellers et al. 1996b); therefore, there is no land use change in the experiments. Grid cells in the Amazon forest are designated as tropical broadleaf evergreen forest, and NDVI is held constant at the maximum value during the measurement period. The use of a constant NDVI avoids known errors in the remotely sensed vegetation index because of cloud and aerosol contamination (Los et al. 2000; Hilker et al. 2012; Samanta et al. 2012). The parameter fPAR is a strong determinant of model potential photosynthesis and transpiration rates, and it saturates above an LAI of 4 m<sup>2</sup> m<sup>-2</sup>. Therefore, the constant NDVI introduces only minor errors in regions with high LAI, as is the case in much of the Amazon basin (Myneni et al. 2007; Malhado et al. 2009; Miller et al. 2004). However, semideciduous forests are common in the transition zone between the evergreen tropical forests and savannas, and in these regions LAI can display strong seasonality. For example, LAI varies from 2–2.5 m<sup>2</sup> m<sup>-2</sup> during the dry season to 5–6 m<sup>2</sup> m<sup>-2</sup> during the wet season at a site northeast of Sinop, Mato Grosso (11°24.75'S, 55°19.50'W) (Vourlitis et al. 2011). In these regions, SiB3 will likely overestimate dry season ET as a result of the constant LAI and fPAR.

SiB3 constrains the net ecosystem exchange (NEE) of CO<sub>2</sub> to be roughly zero each year, since the model does not include dynamic vegetation or biomass storage and cannot accumulate or lose carbon. NEE is not exactly zero because the respiration is based on the previous year's assimilation. Soil texture is based on maps from the International Geosphere-Biosphere Programme (IGBP; Global Soil Data Task Group 2000).

Potential photosynthesis in SiB3 is linearly weighted by three stress factors to give the actual photosynthetic rate. The three factors range from 0.1 (maximum stress) to 1 (no stress) and parameterize the impacts of less than optimal temperature, humidity, and soil moisture on the gross carbon assimilation (Sellers et al. 1992, 1996a). The modifications in SiB3 stressed relate to the soil moisture stress, which at strong water deficits can induce stomatal closure and reduce transpiration and photosynthesis. There are three differences between SiB3 stressed and unstressed (Table 1). First, the soil is 3.5-m deep in SiB3S and 10-m deep in SiB3U. Root depths vary by biome and density decreases exponentially with

TABLE 1. Differences in the model formulation between SiB3 stressed and unstressed.

	SiB3 stressed	SiB3 unstressed
Number of soil layers	10	10
Soil depth (m)	3.5	10
Treatment of root water extraction	Extraction weighted by root biomass.	Extraction weighted by soil moisture in the layer.
Soil moisture stress function	Stress increases linearly with decreasing soil moisture.	Stress increases gradually (slower) with decreasing soil moisture.

depth (Jackson et al. 1996). Roots extend through the entire soil column in both versions in the tropical broadleaf evergreen biome. Second, roots in SiB3U are able to access soil moisture wherever it is in the soil column, regardless of root biomass (Baker et al. 2008). This emphasizes the role of deep roots in efficiently accessing soil moisture. In SiB3S, root water extraction is weighted by biomass, which emphasizes the shallow soil layers over the deep layers. Third, the dependence of soil moisture stress on the volumetric water content is revised, such that SiB3U experiences less stress at moderate soil moisture reductions. For further details of these changes see Baker et al. (2008).

#### b. BUGS5

BUGS5 has evolved from the University of California, Los Angeles (UCLA), GCM to include a geodesic grid and modified sigma coordinate (Suarez et al. 1983; Randall et al. 1985; Ringler et al. 2000) (<http://kiwi.atmos.colostate.edu/BUGS/BUGSoverview.html>). The planetary boundary layer (PBL) depth changes are due to horizontal mass flux divergence, entrainment, and convective mass flux. The entrainment rate is predicted by integrating the turbulent kinetic energy (TKE) conservation equation over the depth of the PBL (Denning et al. 2008). BUGS5 uses a modified Arakawa–Schubert cumulus parameterization with a prognostic cumulus kinetic energy (Ding and Randall 1998; Pan and Randall 1998), which relaxes the quasi-equilibrium closure of the model’s original Arakawa–Schubert parameterization. The stratiform parameterization includes prognostic variables for cloud water, cloud ice, rain, snow, and water vapor (Fowler et al. 1996) and is directly coupled to the cumulus parameterization. The microphysical parameterization follows Fowler and Randall (2002). The radiation scheme is adopted from the National Center for Atmospheric Research (NCAR)’s Community Atmosphere Model (CAM), which uses

a 2-stream method for calculating broadband and heating rates in the shortwave and longwave and accounts for infrared scattering (Gabriel et al. 2001; Stephens et al. 2001).

The dynamical core is based on a spherical geodesic grid (Ringler et al. 2000), which solves the vorticity and divergence equations with second-order accuracy. The model resolution is 10 242 grid cells, which yield an average cell area of  $4.98 \times 10^{-4} \text{ km}^2$  (for comparison a  $2.5^\circ \times 2.5^\circ$  grid has 10 368 grid cells). BUGS and an earlier version of SiB3 (SiB2) were initially coupled in the early 1990s (Randall et al. 1996; Denning et al. 1996), and SiB3 was tested in a single column version of BUGS5 (Harper et al. 2010). In the present study, we ran SiB3U and SiB3S coupled to BUGS5 with observed SSTs from 1997 to 2006. The SSTs are from the Program for Climate Model Diagnosis and Intercomparison (PCMDI) as part of the Atmospheric Model Intercomparison Project (AMIP) Phase II (Taylor et al. 2000; Hurrell et al. 2008). We ran five 10-yr ensembles of each version of the model, each initialized with a restart file from a previous, spunup AMIP-style run created in the first 5 days of 1997 (ensemble 1 begins with the 1 January restart, ensemble 2 begins with the 2 January restart, etc.). The biome maps for SiB3 are identical for the two runs; therefore, the only differences are the changes in Table 1.

#### c. Datasets and analysis

A number of datasets are used for comparison with model results. First, the National Centers for Environmental Prediction–U.S. Department of Energy (NCEP–DOE) Reanalysis, version 2 (NCEP2; Kalnay et al. 1996), was provided by the National Oceanic and Atmospheric Administration (NOAA) Earth System Research Laboratory’s Physical Sciences Division (from their website at <http://www.esrl.noaa.gov/psd/>). We limit our use of NCEP2 to the observation-based variables air temperature, relative humidity, vertical velocity  $\omega$ , and geopotential height. Precipitation is from the Global Precipitation Climatology Project (GPCP) version 2.1 (Adler et al. 2003), and the outgoing longwave radiation (OLR) is from the Earth’s Radiation Budget Experiment (ERBE), which based OLR on observations from the Earth’s Radiation Budget Satellite and the *NOAA-9* and *NOAA-10* satellites from February 1985 to April 1989. (ERBE data were accessed at <http://www2.cgd.ucar.edu>.) The NCAR command language (NCL 2013) was used for much of the analysis (e.g., significance testing) and plotting. Statistical significance of differences between the models is determined with two-tailed Student’s *t* test. If the returned probability is less than 0.05, we reject the null hypothesis that the means

are from the same population; hence, the differences are significant.

To diagnose behavior during dry season droughts, we first computed an area-averaged time series of precipitation from 9°–14°S, 50°–60°W, considering tropical forest points only (see Fig. S1 in the supplementary material; box in Fig. 3). This region contains the largest differences in surface fluxes between SiB3 stressed and unstressed, and it encompasses the transition between the humid tropical forests and the more arid savannas. Within this region, the dry season lasts from May through September. The average seasonal cycle was removed to avoid a seasonal bias when determining drought months, and we applied a 5-month running mean to remove short-lived precipitation anomalies. The resultant anomaly time series is shown in Fig. S2 of the supplemental material, and we defined dry season droughts for each ensemble as austral winter months [June–August (JJA)] with precipitation anomalies  $< -1$ . Composites of drought conditions in each ensemble were then averaged together for analysis of land–atmosphere interactions.

We also determined drought months using two well-known drought indices: the standardized precipitation index (SPI) (McKee et al. 1993; Taylor et al. 2012) and the soil moisture anomaly (SMA) (e.g., Burke and Brown 2008). The SPI was calculated by fitting a gamma distribution to the precipitation time series in Fig. S1 and standardizing the resultant time series. By definition, the SPI3 is based on anomalies from the preceding 3 months and highlights short-term droughts, while the SPI6 is based on the previous 6 months and identifies longer-term (but subannual) droughts. We calculated the SPI for each ensemble and determined drought months (during JJA only) as summarized in Table 2. The SMA is directly related to the soil moisture stress felt by the model:

$$\text{SMA} = \text{SM} - \text{SM}_c, \quad (1)$$

where SM is the soil moisture content for the entire rooting profile averaged over the preceding 12 months, and  $\text{SM}_c$  is the soil moisture climatology for the individual ensemble. The SMA was standardized, and we defined droughts as months (during JJA) when the  $\text{SMA} < -1$ .

### 3. Evaluation of BUGS5 climatology

#### a. Global climatology

The overall patterns of modeled climate agree well with observations, and the global climate is roughly

TABLE 2. Methods for defining dry season drought months. In each case the time series refers to the area-averaged precipitation over the SE Amazon region, as shown in Fig. 3.

Method	Description
Anomaly time series	Standardized anomalies from the deseasonalized time series with 5-month running mean.
SPI3	Standardized precipitation index based on the previous 3 months.
SPI6	Standardized precipitation index based on the previous 6 months.
SPI: very extreme	$-2.00 > \text{SPI}$
SPI: extreme	$-1.60 > \text{SPI} > -1.99$
SPI: severe	$-1.30 > \text{SPI} > -1.59$
SPI: moderate	$-0.80 > \text{SPI} > -1.29$
SPI: abnormally dry	$-0.51 > \text{SPI} > 0.79$
SMA	Soil moisture anomalies based on the annual soil moisture.

similar in BUGS5 with SiB3U and SiB3S (Fig. S3 in the supplementary material). In general, the model tends to produce overvigorous precipitation at the expense of growing high clouds, as indicated by globally high biases in precipitation and OLR. During July, BUGS5 captures observed patterns of global precipitation, but the global mean is too high because of the overestimations in tropical convergence zones (Fig. S3). Modeled OLR is higher than the global observed average, indicating an underestimation of cloud cover, especially for high clouds. Previous work with BUGS showed the sensitivity of tropical rainfall to the parameter  $\alpha$  in the cumulus parameterization (Lin et al. 2000). The cloud mass flux is inversely proportional to the  $\sqrt{\alpha}$  (Pan and Randall 1998). This study uses the default value of  $\alpha = 10^8$  but a larger value might yield more realistic precipitation throughout the tropics (Lin et al. 2000). Precipitable water is also too high in most of the tropics (not shown). Global-mean temperature is slightly higher in BUGS5 than in the NCEP2 reanalysis, mostly due to overestimation in subtropical dry zones (such as the Sahara and Arabian Peninsula) and in the midlatitudes (recall that SSTs are set by observed values). Many of the same biases are seen in the January climatology (Fig. S4), and the model performance during January is discussed in the supplementary material.

#### b. Tropical South American climate

Observed annual precipitation has a maximum in the northwestern Amazon (Fig. 1), and high annual rainfall extends to the southeast through the South Atlantic convergence zone. The models capture the mean pattern of high annual rainfall in the northwest and lower rainfall in the southeast. There is too much rainfall in the

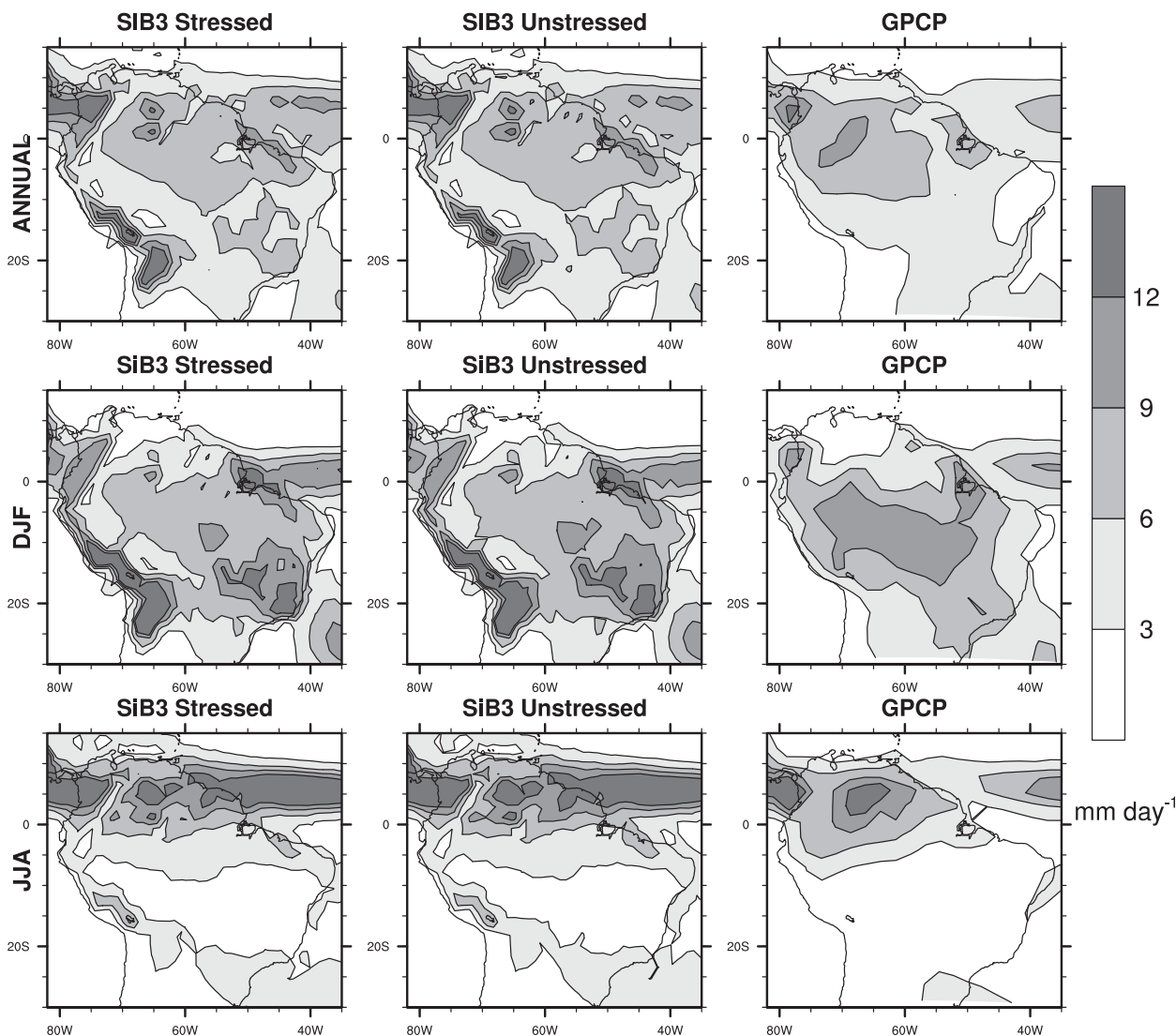


FIG. 1. Average precipitation annually and during DJF and JJA in (left) SiB3S, (center) SiB3U, and (right) GPCP. The models and observations are plotted in their native grid ( $2.5^{\circ} \times 2.5^{\circ}$  for GPCP and roughly  $2.5^{\circ} \times 2.5^{\circ}$  for the models). Time period for averages is 1997–2006.

ITCZ and over high topography, such as the Andes and above southern Brazil. The average precipitation for all tropical forest points in South America is  $6.64$  and  $6.74 \text{ mm day}^{-1}$  in SiB3S and SiB3U, respectively. This is high compared to GPCP ( $P = 5.2 \text{ mm day}^{-1}$ ) but within the range of measurements compiled by Marengo (2006) ( $5.2\text{--}8.6 \text{ mm day}^{-1}$ ).

For the majority of the Amazon, the wet season occurs during December–February (DJF) and the dry season occurs during JJA (Fig. 1). This seasonal cycle is reversed north of the equator. A predominant feature of the lower-atmospheric circulation is the trade winds, which transport low-level moisture from the tropical Atlantic Ocean and Caribbean Sea across the continent

and toward the Andes (Figs. S5a,c in the supplementary material). The highest rainfall occurs in the western Amazon basin, when the Andes force the air southward. During July, winds south of the equator are southeasterly, which limits moisture transport into the southern Amazon compared to the wet season (Fig. S5c). At  $850 \text{ hPa}$ , there is anticyclonic flow off the southern coast of Brazil, and at  $200 \text{ hPa}$ , westerlies dominate the circulation (Fig. S5d). BUGS5 captures these mean circulation patterns well with a few exceptions: exaggeration of the anticyclone at low levels in July [related to the coarsely resolved southeastern (SE) Brazilian highlands] and underestimation of the southerly component of winds in July in the central Amazon.

Average precipitation for South American tropical forests has a similar seasonal cycle in both versions of the model. These are controlled by the large-scale circulation patterns described above. To better understand precipitation biases in the model, we averaged seasonal rainfall over two regions used in an analysis of models from phase 5 of the Coupled Model Intercomparison Project (CMIP5) (Yin et al. 2013): the southern Amazon (SAma: 5°–15°S, 50°–70°W) and northern Amazon (NAma: 5°N–5°S, 55°–70°W) (Fig. S6 in the supplementary material). In the SAma, the models produce dry biases of 2.6 and 2.4 mm day<sup>−1</sup> (in SiB3 stressed and unstressed, respectively) during the wet season (DJF) and wet biases of 1.6 and 1.5 mm day<sup>−1</sup> during the dry season (JJA) (Fig. S6b). The JJA wet bias is in contrast to the majority of the CMIP5 models, which mostly produce a dry bias (Yin et al. 2013). Compared to the European Centre for Medium-Range Weather Forecasts (ECMWF) Interim Re-Analysis (ERA-Interim), the majority of CMIP5 models overestimate dry season moisture divergence in the SAma, possibly related to an overactive ITCZ and strong subsidence over the Amazon. The two models without a dry season dry bias [Hadley Centre Global Environmental Model 2, Carbon Cycle (HadGEM2-CC) and Hadley Centre Global Environmental Model 2, Earth System (HadGEM2-ES)] compensate for high moisture divergence by also having high ET. Following the methodology in Yin et al. (2013), we calculated moisture convergence as

$$MC = P - ET + \Delta TWV, \quad (2)$$

where  $\Delta TWV$  is the monthly change in atmospheric total water vapor. In the SAma, the BUGS5 model demonstrates a similar trade-off between ET and MC as the two Hadley Centre models (Fig. S7). In SiB3 stressed, ET is low and MC is near 0, meaning very small moisture divergence. In SiB3 unstressed, ET is higher by 0.69 mm day<sup>−1</sup>, but  $P$  is slightly lower (by 0.04 mm day<sup>−1</sup>). The excess water vapor originating from ET is transported away from the Amazon, and MC is more negative by 0.73 mm day<sup>−1</sup>. A similar result was found using SiB3 stressed and unstressed coupled to a single column version of BUGS5 (Harper et al. 2010).

In the NAma, observed rainfall is relatively high year-round, but the driest (wettest) months are September–November (SON) [March–May (MAM)] (Fig. S6). The BUGS5 modeled seasonal cycle does not match observations: the driest (wettest) months occur during DJF (SON) in BUGS5. Because of these high biases in the northern Amazon, the focus of the remaining analysis is on the southern Amazon. However, since the mean state of the dry season in the southern Amazon is too wet,

drought intensities and responses might be dampened in these experiments.

## 4. Results

### a. Impact of water stress on dry season fluxes and precipitation

Because of the changes in root zone biophysics (see section 2a; Table 1), SiB3 unstressed avoids moisture-related stress during the dry season. For illustrative purposes, Fig. 2 shows daily averages from the two versions of the model during 1999 at a point in the southern Amazon. During the dry season, the stomatal resistance is lower in SiB3 unstressed, leading to higher rates of photosynthesis and transpiration and therefore higher LH. Because the net surface energy must be balanced, the higher LH results in lower SH. During JJA, there are significant model differences in surface fluxes along the southern edge of the forest (Fig. 3).

We define the region with the largest model differences as the SE Amazon for the purpose of further analysis (9°–14°S, 50°–60°W, tropical forest points only; see box in Fig. 3). (Note that this region is different from the SAma region in section 3.) The dry season is relatively long and dry, lasting from May to September with an average precipitation of 1.3–1.6 mm day<sup>−1</sup> in the models; therefore, the impact of enhanced soil water access is greater than in regions with a less pronounced dry season. Sensible heat flux in SiB3 stressed is more than twice that from SiB3 unstressed (56 compared to 27 W m<sup>−2</sup>) (Table 3), and LH is on average 40% higher in SiB3 unstressed, with the largest difference of 48 W m<sup>−2</sup>. As mentioned in section 2a, LAI and fPAR are prescribed at a constant value in SiB3 and are likely overestimated during the dry season in this region. High LAI could lead to overestimated ET, but this bias is present in both versions of the model.

Enhanced LH could increase rainfall through moistening and destabilizing the lower atmosphere (Fu and Li 2004). The model differences in precipitation are small but significant ( $p < 0.05$ ) (Fig. 3). On average, precipitation in the South American tropical forests is marginally greater in SiB3U (by 0.1 mm day<sup>−1</sup>). Within the SE region, however, precipitation is greater in SiB3S (JJA average 1.95 compared to 1.61 mm day<sup>−1</sup> in SiB3U), with the largest difference of 0.8 mm day<sup>−1</sup>.

Convective activity in the model depends on the atmospheric static stability. In SiB3U, enhanced surface humidity decreases the static stability (because of more latent heat in the low atmosphere), while cooler surface temperatures from reduced SH increase stability. During the average dry season, the latter effect is greater,

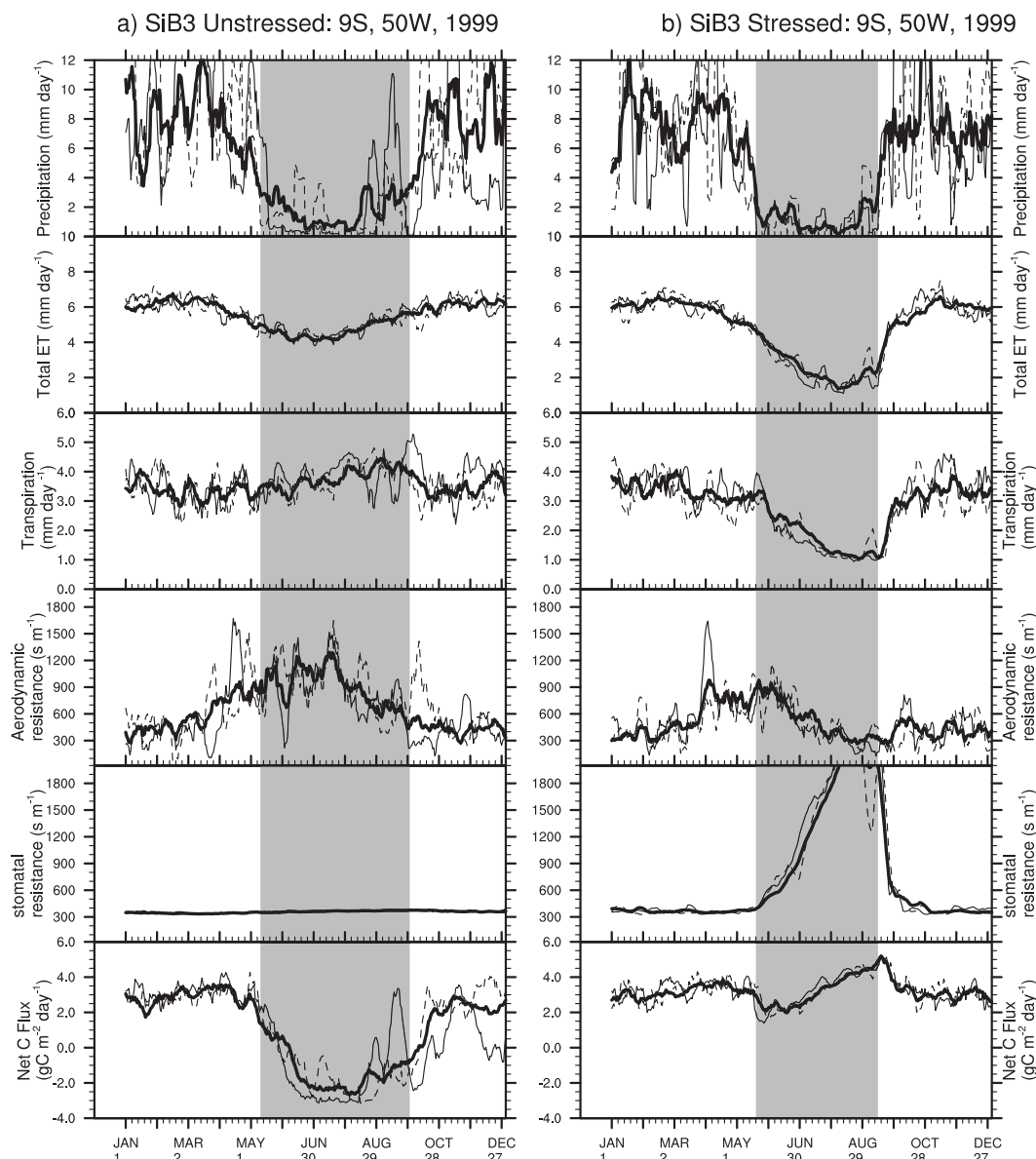


FIG. 2. (top)–(bottom) Precipitation, ET, transpiration, aerodynamic resistance, stomatal resistance, and net carbon flux from the canopy. The dark line is the average of the five ensembles. Patterned lines show the variability seen in individual ensembles: dashed line (ensemble 2) and thin solid line (ensemble 3). All time series have a 10-day running mean applied. Dark shading indicates the dry season in the ensemble average.

and overall the static stability is greater in SiB3U, resulting in reduced CAPE and rainfall compared to SiB3S. We examine these differences in more detail in Fig. 4, which shows both latitude–height cross sections (averages from  $0^{\circ}$ – $15^{\circ}\text{S}$ ,  $50^{\circ}$ – $60^{\circ}\text{W}$ ) and an average vertical profile (from  $11^{\circ}$ – $13^{\circ}\text{S}$ ,  $50^{\circ}$ – $60^{\circ}\text{W}$ ). The largest differences in temperature, RH, and moist static energy  $h$  occur near  $12^{\circ}\text{S}$ , where differences in surface fluxes are the greatest. In the lower atmosphere, SiB3S is roughly 1.5 K warmer than SiB3U, and SiB3U has slightly higher

surface relative humidity (Table 3). However, less of this moist air is transported upward due to large-scale subsidence in SiB3U. The air is slightly warmer and more moist in SiB3S above 700 hPa. The combined effect is higher  $h$  in SiB3S, with significant differences between the models below 600 hPa and south of  $5^{\circ}\text{S}$ .

SiB3S has rising air in the low atmosphere, while SiB3U has subsiding air throughout the profile. In comparison, this region is characterized by subsidence in the NCEP2 reanalysis (bearing in mind that in data-sparse regions



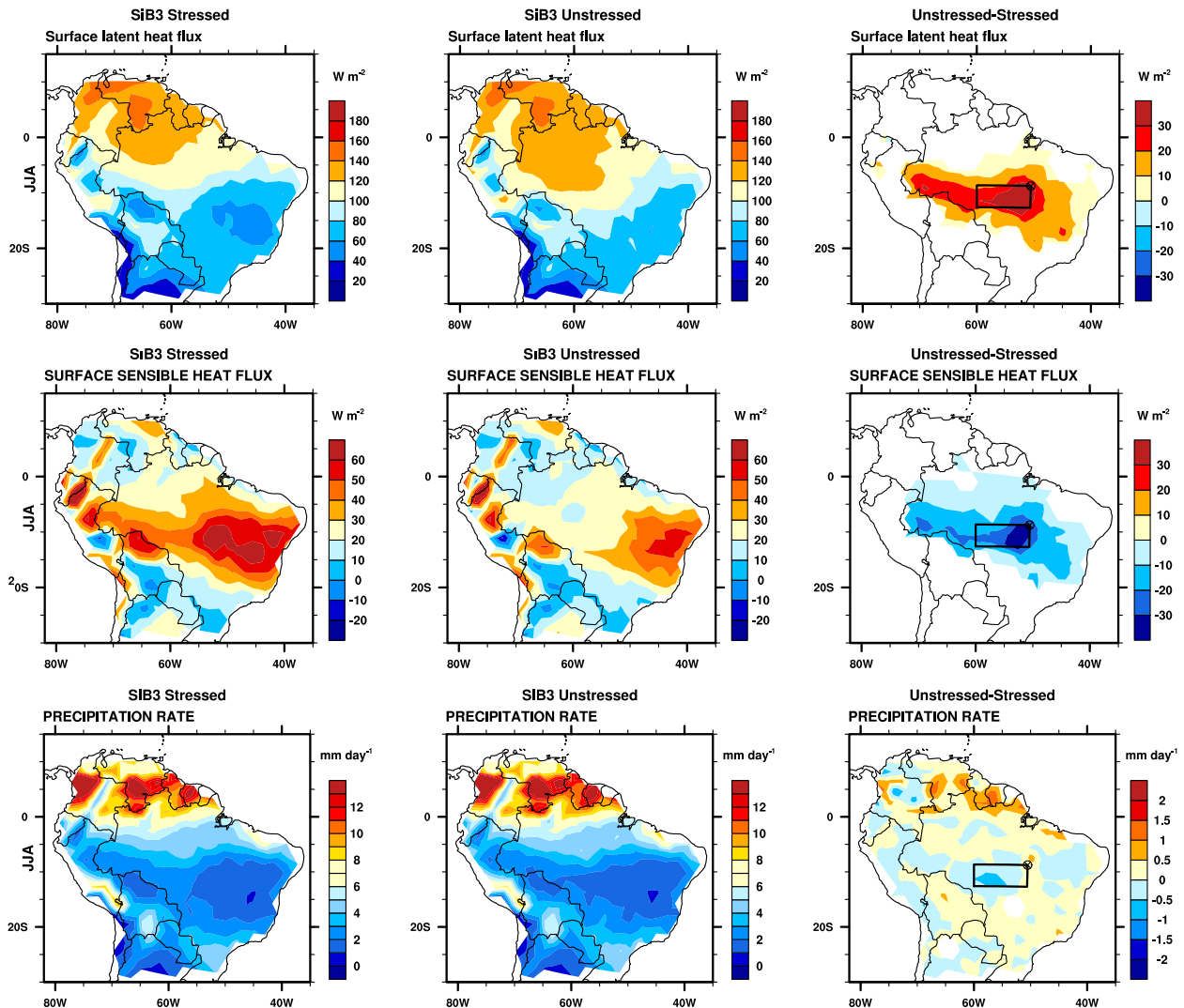


FIG. 3. (top) LH ( $\text{W m}^{-2}$ ), (middle) SH ( $\text{W m}^{-2}$ ), and (bottom) precipitation ( $\text{mm day}^{-1}$ ) during JJA in (left) SiB3S, (center) SiB3U, and (right) the difference between the models (unstressed – stressed). Only significant differences are shown ( $p < 0.05$ ). The box over the SE Amazon region is discussed in the text ( $9^{\circ}$ – $14^{\circ}\text{S}$ ,  $50^{\circ}$ – $60^{\circ}\text{W}$ ). The circle in the top right of the box marks the location used in Figs. 2 and 9.

such as the Amazon, reanalysis products rely heavily upon a model to fill in gaps between observations). The NCEP2 profile is slightly cooler and drier than the modeled profiles (and RH is much lower), resulting in lower  $h$ . This is consistent with the result of BUGS5 overestimating dry season precipitation. Compared to the observations, the tendency toward subsidence and lower precipitation rates in SiB3U is an improvement, although a large bias in atmospheric RH still exists.

#### *b. Land–atmosphere interactions during dry season droughts*

The following discussion focuses on the previously defined SE Amazon region ( $9^{\circ}$ – $14^{\circ}\text{S}$ ,  $50^{\circ}$ – $60^{\circ}\text{W}$ ), where

dry season differences in surface fluxes are most pronounced. Over this region, we defined dry season droughts as explained in Table 2, first exploring composites based on the simple anomaly time series. During an average dry season, winds at 850 hPa are predominantly easterly above the central Amazon basin in the NCEP2 reanalysis, and there is anticyclonic rotation above southern Brazil (Fig. S5). During modeled dry season droughts, this flow is reversed: the 850-hPa winds are anomalously southeasterly above southern Brazil, and westerly near the equator (Fig. 5). Instead of moist air flowing onto the continent from the tropical Atlantic, drier air is advected into the Amazon region from the south-southeast. The atmosphere is warmer and drier

TABLE 3. Average latent heat, sensible heat, Bowen ratio (SH/LH), precipitation, temperature at 850 hPa ( $T_{850}$ ), and specific humidity at 850 hPa ( $q_{850}$ ) during an average JJA and during dry season droughts.

	SiB3S (JJA)	SiB3U (JJA)	SiB3S (drought)	SiB3U (drought)
LH ( $\text{W m}^{-2}$ )	77	114	63	112
SH ( $\text{W m}^{-2}$ )	56	27	65	32
BR	0.72	0.24	1.03	0.29
$P$ ( $\text{mm day}^{-1}$ )	1.95	1.61	1.29	1.57
$T_{850}$ (K)	292.1	290.8	292.0	290.8
$q_{850}$ ( $\text{kg kg}^{-1}$ )	0.0122	0.0125	0.0108	0.0122

than during an average dry season, and the differences in surface fluxes between the models are enhanced (Fig. 6; Table 3).

Contrary to the results for an average dry season, the enhanced ET in SiB3U can play an important role in moisture recycling during dry season droughts. Precipitation in the SE Amazon region is approximately 20% higher in SiB3U (Fig. 6; Table 3). The unstressed atmosphere is cooler (by up to 1.8 K at 850 hPa) and more moist (by on average  $1 \text{ g kg}^{-1}$ ). The result is slightly higher  $h$  between the surface and 850 hPa, although the differences are not significant (Fig. 7). The moist static energy is higher near the surface and lower near 700 hPa, and there is slightly more CAPE in SiB3U. Above 700 hPa, subsidence is stronger in SiB3S.

Although rainfall during droughts is higher in SiB3U, the number of drought months is also higher. This is likely a result of the selection criteria. During the dry season, the modeled rainfall is infrequent but heavy rains are possible, leading to a bimodal probability distribution for dry season rain rates in both versions of the model. In SiB3U this distribution is spread out: the very dry and very wet months are more frequent at the expense of average months (Fig. S8 in the supplementary material). Therefore, it is more likely for this model to encounter dry season months with low rain rates. To test the dependence of results on the definition of drought months, we composite dry season droughts based on the SPI and SMA (Table 2). There are more drought months during JJA using these two indices than with the original index. The timing of droughts in the original index is most similar to the 3-month SPI. The annual SMA best captures the long-term nature of the 2005 drought in the SE Amazon region, which was particularly severe because it followed an anomalously dry wet season (Marengo et al. 2008a). The model simulates drought conditions during the austral winter of 2005 in three of the five ensembles for SiB3 stressed and in four of the five ensembles for SiB3 unstressed.

During droughts based on the SPI, the average precipitation over the SE Amazon region is higher in the model with higher RH throughout the profile and higher vertically integrated  $h$  (Figs. 8 and S9). An additional

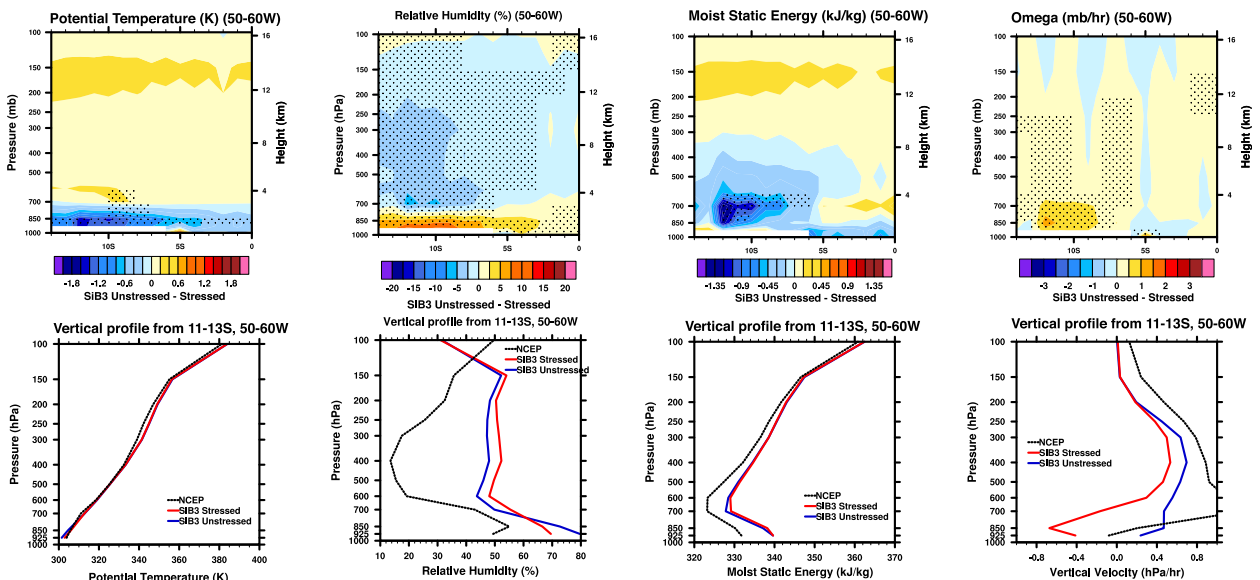


FIG. 4. (top) Latitude–height cross sections of model differences (SiB3U – SiB3S) of potential temperature (K), RH (%),  $h$  ( $\text{kJ kg}^{-1}$ ), and  $\omega$  ( $\text{hPa hr}^{-1}$ ) from 0° to 15°S (averaged from 50° to 60°W) during JJA. Stippling indicates regions of significant differences between the models ( $p < 0.05$ ). (bottom) Vertical profiles averaged over 11°–13°S and 50°–60°W from the two models and NCEP2 reanalysis.

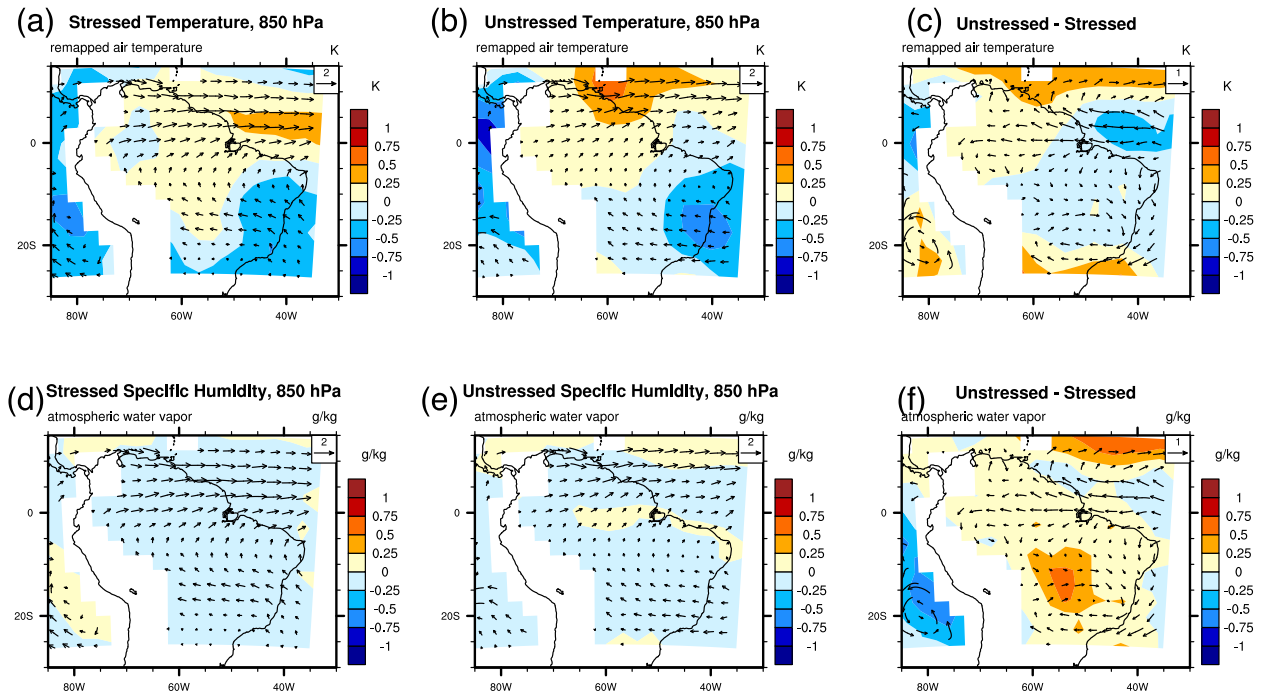


FIG. 5. Composites of anomalous 850-hPa winds, (a)–(c) temperature, and (d)–(f) specific humidity during JJA droughts (as defined with the anomaly time series) in (a),(d) SiB3S, (b),(e) SiB3U, and (c),(f) the difference between the two models.

factor is the BR in SiB3 stressed (Table 4). The BR for SiB3 unstressed is always between 0.25 and 0.35, and it is always higher in SiB3 stressed (0.8–1.3). When  $BR > 1$  in SiB3 stressed, the model differences in lower-atmospheric moisture are substantial, leading to stronger moisture recycling in SiB3 unstressed. For example, during extreme and moderate droughts as defined with the 6-month SPI,  $BR > 1$  in SiB3S, and lower-atmospheric RH and  $h$  are both higher in SiB3U (Fig. 8). As a result, precipitation is stronger in SiB3U (Table 4). Conversely, when  $BR < 1$  in SiB3S during severe droughts and abnormally dry periods, the lower atmosphere's  $h$  is higher and precipitation is higher than in SiB3U. Similar relationships between surface fluxes in SiB3 stressed and precipitation are seen with the 3-month SPI (see the supplemental material). Droughts defined with the SMA are generally less severe than the SPI droughts. The vertical structures of model differences in RH,  $h$ , and  $\omega$  are similar to those during an average JJA (Fig. S10). There is more moist static energy in the lower atmosphere in SiB3S, and stronger precipitation in this model (Table 4).

### c. Case study

Next we analyze the dry season land–atmosphere interactions at 9°S, 50°W, which is a tropical forest point near the forest–savanna transition (see Fig. 3). While the

previous analysis focused on large-scale patterns, this allows more detailed investigation of weekly variability in surface energy fluxes and their impact on the overlying circulation. We purposefully use an area near the forest–savanna transition because it is impacted by more arid air, which increases evaporative demand and intensifies the difference in LH between the models. During the average dry season, plants are able to draw on stored soil moisture in both models. Modeled ET rates decline during July, similar to the observed seasonal cycle from a nearby tower (Javaes; da Rocha et al. 2009). However, there are two complications with directly comparing the model results to in situ observations. First, the wet bias during JJA results in low moisture stress in both versions of the model. Average modeled dry season precipitation was 100–106 mm month<sup>−1</sup>, while observed precipitation near Sinop (11°24.75'S, 55°19.50'W) was 50–100 mm month<sup>−1</sup> (Vourlitis et al. 2011). Second, the SiB3 input data classify the region as tropical broadleaf evergreen biome, while the true vegetation coverage is a semideciduous forest (Vourlitis et al. 2011; Costa et al. 2010; Lathuilliere et al. 2012). The semideciduous forests typically have a dry season decrease in ET due to both phenology and stomatal control (Costa et al. 2010; Vourlitis et al. 2011). Although SiB3 unstressed simulates a dry season increase in aerodynamic

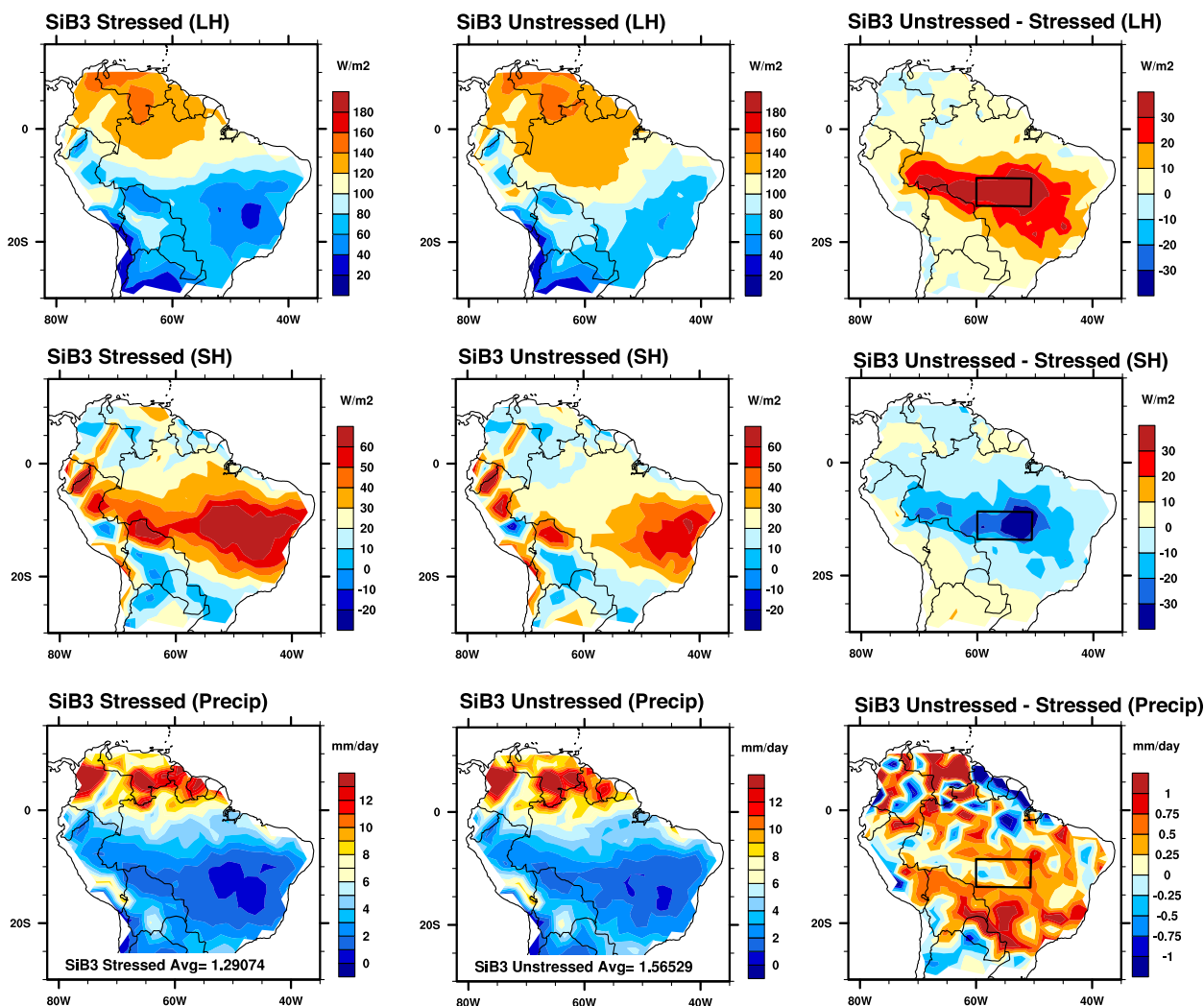


FIG. 6. As in Fig. 3, but for averages are during dry season drought months. Note that all differences are shown.

resistance, the stomatal resistance shows almost no seasonal cycle (Fig. 2). Therefore, it is likely that the unstressed model overestimates dry season ET at this point, and the model differences in this section can be viewed as representing two extremes in land-atmosphere interactions.

In SiB3S, canopy transpiration declines throughout the dry season, and the PBL is warmer and drier. During a simulated dry season drought (1999), transpiration is below average in both models, but LH is lower by up to  $60 \text{ W m}^{-2}$  in SiB3S (Fig. 9). The LH is closely linked to rainfall events in SiB3S, while SiB3U produces a higher flux with less variability. As a result, the atmospheric precipitable water (PRW) remains relatively low in SiB3S through mid-August, while both PRW and  $h$  increase about a month earlier in SiB3U. Although both versions of the model simulate

a drought, the anomalously dry conditions last longer in SiB3S.

Figure 9 also shows results from two ensembles. In ensemble 2 (dashed line), SiB3U's LH is fairly steady through June and isolated rainfall events keep the monthly-mean precipitation high. Precipitable water is similar in the two models until mid-July, when continued dry conditions result in low LH in SiB3S. Latent heat flux reaches a minimum by mid-July, and PRW,  $h$ , and CAPE also experience strong reductions. The average rainfall during July is  $0.39 \pm 0.26 \text{ mm day}^{-1}$  in SiB3S compared to  $1.62 \pm 1.08 \text{ mm day}^{-1}$  in SiB3U. Alternatively, SiB3U produces less rainfall than SiB3S during June–July 1999 in ensemble 3. In this case, large-scale dry conditions overshadow the higher LH in SiB3U and result in low CAPE, PRW, and  $h$ . This represents a limit on the moisture recycling capacity of the forest.

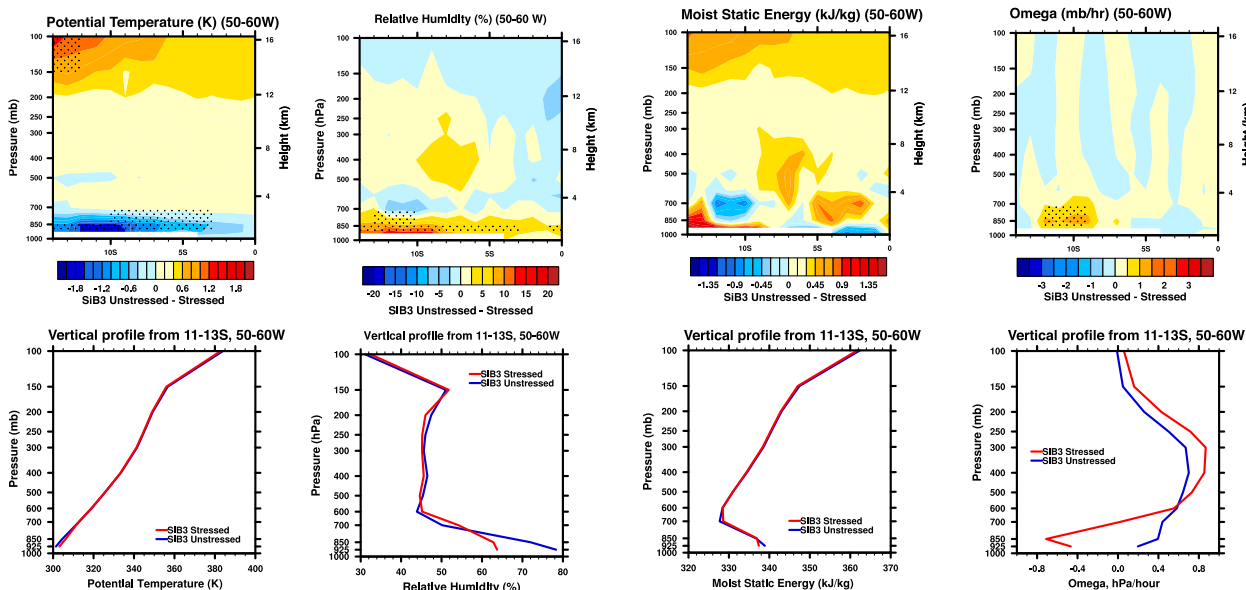


FIG. 7. As in Fig. 4, but during JJA droughts.

The differences in soil moisture access between the models also have implications for the carbon cycle. The net  $\text{CO}_2$  flux from the canopy to the atmosphere is the difference between uptake by the forest through photosynthesis and efflux resulting from respiration (the convention in Fig. 9 is such that a negative flux is uptake).

SiB3U generally simulates the land as a carbon sink during the dry season of 1999 because of higher rates of photosynthesis than respiration, while the opposite is true for SiB3S. Localized precipitation events can temporarily switch the carbon sink to a source. For example, in ensemble 3, large pulses of soil respiration following

### JJA Droughts defined from SPI6 (differences = Unstressed - Stressed)

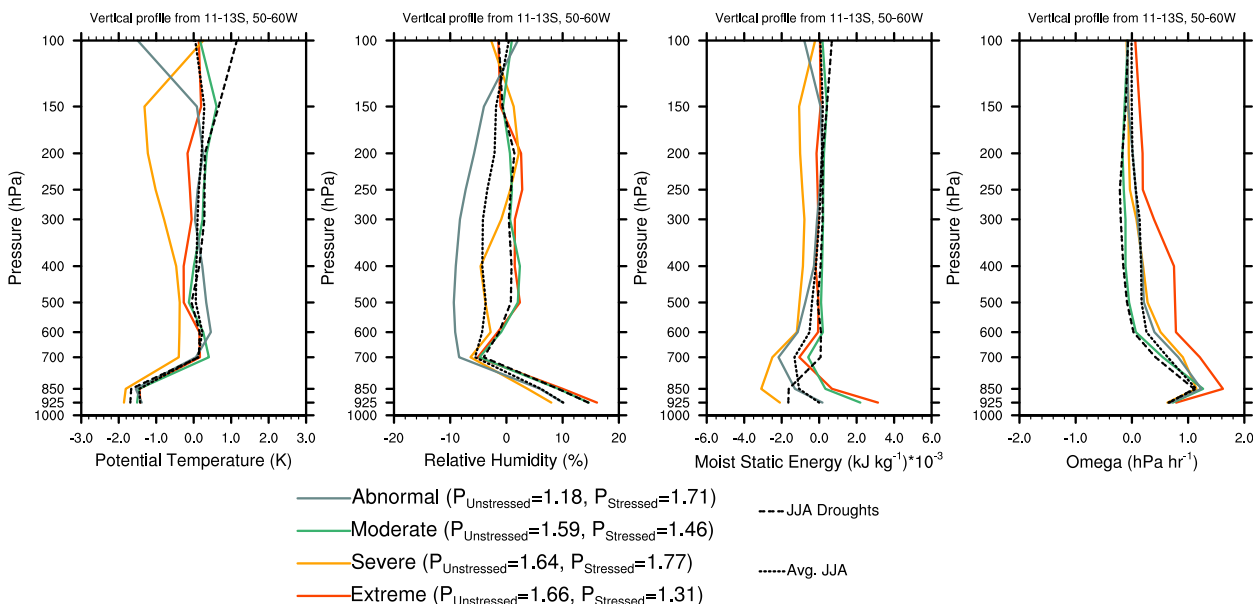


FIG. 8. Differences (SiB3U – SiB3S) in the vertical profiles during droughts defined from the 6-month SPI. Profiles are averaged over 11°–13°S, 50°–60°W. Drought intensities are defined in Table 3. For reference the profiles are shown for an average JJA and a JJA drought defined with the anomaly time series.

TABLE 4. Model differences during an average dry season and during dry season droughts as defined by the original anomaly time series, the SMA, and the SPI. The BR is shown as the value for SiB3 stressed only. Only drought composites are shown for which  $>2$  months of drought occurred in each model:  $\Delta P = (P_{\text{SiB3U}} - P_{\text{SiB3S}}) / P_{\text{SiB3S}}$ ,  $\Delta q = q_{850, \text{SiB3U}} - q_{850, \text{SiB3S}}$ , and  $\Delta T = T_{850, \text{SiB3U}} - T_{850, \text{SiB3S}}$ .

	Average	Anomaly time series		SMA
BR	0.72	1.03		0.8
$\Delta T$ (K)	-1.3	-1.2		-1.4
$\Delta q$ (g kg <sup>-1</sup> )	0.3	1.4		0.6
$\Delta P$	-17%	22%		-11%
	Extreme	Severe	Moderate	Abnormal
3-month SPI				
BR	1.29	0.79	0.94	0.89
$\Delta T$ (K)	-1.2	-1.3	-1.7	-1.6
$\Delta q$ (g kg <sup>-1</sup> )	1.0	0.4	0.8	0.3
$\Delta P$	22%	-8%	-31%	-1%
6-month SPI				
BR	1.2	0.82	1.05	0.69
$\Delta T$ (K)	-1.3	-1.6	-1.3	-1.4
$\Delta q$ (g kg <sup>-1</sup> )	1.3	0.0	1.2	0.3
$\Delta P$	26%	-7%	9%	-30%
12-month SPI				
BR	—	—	0.78	0.93
$\Delta T$ (K)	—	—	-1.5	-1.3
$\Delta q$ (g kg <sup>-1</sup> )	—	—	0.6	1.0
$\Delta P$	—	—	-13%	1%

heavy rains in late August temporarily convert the forest to a carbon source in SiB3U.

## 5. Conclusions

Access to deep soil moisture by efficient rooting systems is important for drought survival (Nepstad et al. 1994, 2007; Jipp et al. 1998). The current study investigates how the avoidance of dry season water stress can increase moisture recycling and mitigate drought intensity. Accounting for drought tolerance mechanisms in SiB3U enables a more realistic simulation of the average dry season in the southern Amazon. Increased LH and reduced SH in SiB3U cool the lower atmosphere, thereby increasing the static stability and reducing convection. The result is somewhat unexpected, since SiB3U has significantly higher ET than SiB3S and a more moist lower atmosphere. There is no evidence for a positive feedback between low precipitation and reduced ET during the average dry season, since SiB3S has lower ET and yet more precipitation.

During a dry season drought, maintained ET has the potential to dampen the drought's intensity if the moistening effect of higher LH is stronger than the cooling effect of lower SH. Precipitation is higher in SiB3U during dry season droughts when the atmospheric conditions are

amenable to convection, as indicated by high relative humidity and moist static energy relative to SiB3S. Additionally when sensible heat flux is higher than latent heat flux in SiB3S, the hot and dry lower atmosphere limits the precipitation relative to SiB3U.

Two factors could limit moisture recycling during drought. First, enhanced moisture availability cannot override a strongly statically stable atmosphere, as was shown to be the case in the example from Ensemble 3 (Fig. 9). In this case, the moist static energy, CAPE, and precipitable water vapor all are anomalously low in SiB3U (even compared to the average during a drought). This is a similar result to the observed impacts of LH on wet season onset from Fu and Li (2004). In that study, which was based on ECMWF reanalysis, an anomalously wet surface was shown to be a necessary but not sufficient condition for early transition from the wet to dry season.

A second factor affecting moisture recycling during drought is the diversity of plant response to drought. Given the high species diversity of the Amazon forest, its trees likely employ a variety of mechanisms for drought tolerance and the avoidance of hydraulic failure. In addition, the modeling study does not account for semideciduous trees in the southern Amazon, nor land use change. Because of these limitations, the response from SiB3 unstressed can be interpreted as an upper limit to the ability of the forest to recycle precipitation. Rainfall exclusion studies have illuminated drought responses in two equatorial Amazon sites, but modeling the subtleties of these responses presents many challenges (e.g., Powell et al. 2013). The current study does not incorporate spatial heterogeneity in drought response, but future model development in Amazonia should account for gradients in plant and soil hydraulic and physiological responses to drought, which could be a function of soil type, rainfall variability, and/or nutrient availability. Continued observations of forest response to drought are essential for such work to move forward.

During particularly strong and/or long droughts, trees reach a limit in their ability to access and use soil moisture. Observational evidence suggests that such a threshold has been reached during droughts in the past decade (Phillips et al. 2010; Lewis et al. 2011). In terms of moisture recycling, it appears there is a threshold in the model that occurs when the Bowen ratio is greater than one. Although this study did not directly address land use change, an important implication is that forest preservation is essential for enabling the Amazon forest to withstand a potentially drier climate. Pasture and secondary forests do not have the extensively developed rooting systems present in primary forest, and loss of



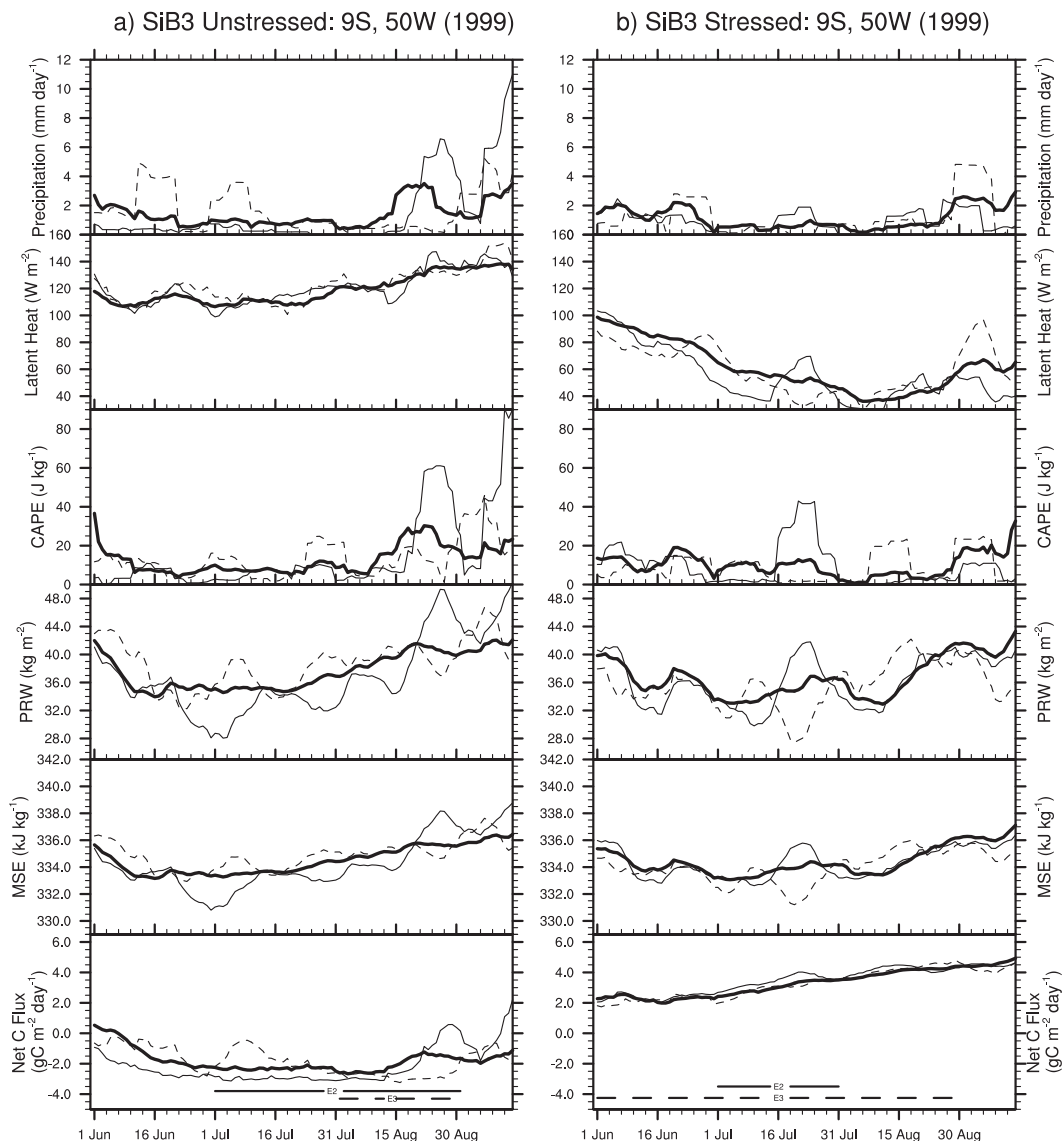


FIG. 9. (top)–(bottom) Precipitation, LH, CAPE, total column PRW, vertically integrated moist static energy (MSE; from 1000 to 100 hPa), and net carbon flux from the canopy during the dry season of 1999. The dark line is the average of five ensembles. Patterned lines show the variability seen in individual ensembles: dashed line (ensemble 2) and thin solid line (ensemble 3). All time series have a 10-day running mean applied. The climatological dry season is May–September. The months that qualified as droughts were July–August (SiB3U, ensemble 2), August (SiB3U, ensemble 3), July (SiB3S, ensemble 2), and June–August (SiB3S, ensemble 3). The beginning and end of the droughts are denoted with the horizontal lines above the  $x$  axis.

vegetation coverage increases runoff during heavy rain. Pasture is more likely to experience dry season water stress and seasonal reductions in ET, particularly in the southern Amazon (von Randow et al. 2012), and deforestation can reduce moisture recycling and downwind precipitation (Spracklen et al. 2012). In addition, forests that border pasture or savanna are more prone to desiccation and fire impacts (Malhi et al. 2008). Large areas of undisturbed forest are more likely to maintain ET during dry periods and recycle rainfall.

**Acknowledgments.** This work was funded through the National Science Foundation's Science and Technology Center for Multiscale Modeling of Atmospheric Processes, managed by Colorado State University under Cooperative Agreement ATM-0425247, and through the U.K. National Environment Research Council Joint Weather and Climate Research Programme. Computing resources were supplied by the National Energy Research Scientific Computing Center, supported by the Office of Science of the U.S. Department of Energy

under Contract DE-AC02-05CH11231. The authors thank the editor, Dr. Michael Coe, and three anonymous reviewers for their helpful reviews of the manuscript.

## REFERENCES

- Adler, R. F., and Coauthors, 2003: The Version-2 Global Precipitation Climatology Project (GPCP) monthly precipitation analysis (1979–present). *J. Hydrometeorol.*, **4**, 1147–1167.
- Aragao, L., Y. Malhi, N. Barbier, A. Lima, Y. Shimabukuro, L. Anderson, and S. Saatchi, 2008: Interactions between rainfall, deforestation and fires during recent years in the Brazilian Amazonia. *Philos. Trans. Roy. Soc. London*, **B363**, 1779–1785.
- Baker, I. T., L. Prihodko, A. S. Denning, M. Goulden, S. Miller, and H. R. da Rocha, 2008: Seasonal drought stress in the Amazon: Reconciling models and observations. *J. Geophys. Res.*, **113**, G00B01, doi:10.1029/2007JG000644.
- , and Coauthors, 2013: Surface ecophysiological behavior across vegetation and moisture gradients in tropical South America. *Agric. For. Meteorol.*, **182–183**, 177–188.
- Burke, E. J., and S. J. Brown, 2008: Evaluating uncertainties in the projection of future drought. *J. Hydrometeorol.*, **9**, 292–299.
- Chen, Y., and Coauthors, 2011: Forecasting fire season severity in South America using sea surface temperature anomalies. *Science*, **334**, 787–791, doi:10.1126/science.1209472.
- Collatz, G., J. Ball, C. Grivet, and J. Berry, 1991: Physiological and environmental regulation of stomatal conductance, photosynthesis and transpiration: A model that includes a laminar boundary layer. *Agric. For. Meteorol.*, **54**, 107–136.
- , M. Ribas-Carbo, and J. Berry, 1992: Coupled photosynthesis-stomatal conductance model for leaves of C4 plants. *Aust. J. Plant Physiol.*, **19**, 519–538.
- Costa, M. H., M. C. Biajoli, L. Sanches, A. C. M. Malhado, L. R. Hutyrá, H. R. da Rocha, R. G. Aguiar, and A. C. de Araujo, 2010: Atmospheric versus vegetation controls of Amazonian tropical rain forest evapotranspiration: Are the wet and seasonally dry rain forests any different? *J. Geophys. Res.*, **115**, G04021, doi:10.1029/2009JG001179.
- Cox, P. M., and Coauthors, 2008: Increasing risk of Amazonian drought due to decreasing aerosol pollution. *Nature*, **453**, 212–215.
- da Rocha, H. R., and Coauthors, 2009: Patterns of water and heat flux across a biome gradient from tropical forest to savanna in Brazil. *J. Geophys. Res.*, **114**, G00B12, doi:10.1029/2007JG000640.
- Denning, A. S., G. J. Collatz, C. G. Zhang, D. A. Randall, J. A. Berry, P. J. Sellers, G. D. Colello, and D. A. Dazlich, 1996: Simulations of terrestrial carbon metabolism and atmospheric CO<sub>2</sub> in a general circulation model. 1. Surface carbon fluxes. *Tellus*, **48B**, 521–542.
- , N. Zhang, C. Yi, M. Branson, K. Davis, J. Kleist, and P. Bakwin, 2008: Evaluation of modeled atmospheric boundary layer depth at the WLEF tower. *Agric. For. Meteorol.*, **148**, 206–215.
- Ding, P., and D. A. Randall, 1998: A cumulus parameterization with multiple cloud base levels. *J. Geophys. Res.*, **103** (D10), 11 341–11 353.
- Eltahir, E. A. B., and R. L. Bras, 1994: Precipitation recycling in the Amazon basin. *Quart. J. Roy. Meteor. Soc.*, **120**, 861–880.
- Espinoza, J. C., J. Ronchail, J. L. Guyot, C. Junquas, P. Vauchel, W. Lavado, G. Drapeau, and R. Pombosa, 2011: Climate variability and extreme drought in the upper Solimões River (western Amazon basin): Understanding the exceptional 2010 drought. *Geophys. Res. Lett.*, **38**, L13406, doi:10.1029/2011GL047862.
- Farquhar, G. D., S. von Caemmerer, and J. Berry, 1980: A biochemical model of photosynthetic CO<sub>2</sub> assimilation in leaves of C<sub>3</sub> species. *Planta*, **149**, 78–90.
- Fisher, R. A., M. Williams, R. L. Do Vale, A. L. Da Costa, and P. Meir, 2006: Evidence from Amazonian forests is consistent with isohydric control of leaf water potential. *Plant Cell Environ.*, **29**, 151–165.
- Fowler, L. D., and D. A. Randall, 2002: Interactions between cloud microphysics and cumulus convection in a general circulation model. *J. Atmos. Sci.*, **59**, 3074–3098.
- , —, and S. A. Rutledge, 1996: Liquid and ice cloud microphysics in the CSU general circulation model. Part I: Model description and simulated microphysical processes. *J. Climate*, **9**, 489–529.
- Fu, R., and W. Li, 2004: The influence of the land surface on the transition from dry to wet season in Amazonia. *Theor. Appl. Climatol.*, **78**, 97–110.
- Gabriel, P. M., P. T. Partain, and G. L. Stephens, 2001: Parameterization of atmospheric radiative transfer. Part II: Selection rules. *J. Atmos. Sci.*, **58**, 3411–3423.
- Global Soil Data Task, 2000: Global soil data products (IGBP-DIS). International Geosphere-Biosphere Programme, Data and Information System, CD-ROM. [Available online at <http://www.daac.ornl.gov>.]
- Harper, A. B., A. S. Denning, I. T. Baker, M. D. Branson, L. Prihodko, and D. A. Randall, 2010: Role of deep soil moisture in modulating climate in the Amazon rainforest. *Geophys. Res. Lett.*, **37**, L05802, doi:10.1029/2009GL042302.
- Hasler, N., and R. Avissar, 2007: What controls evapotranspiration in the Amazon basin? *J. Hydrometeorol.*, **8**, 380–395.
- Hilker, T., A. I. Lyapustin, C. J. Tucker, P. J. Sellers, F. G. Hall, and Y. Wang, 2012: Remote sensing of tropical ecosystems: Atmospheric correction and cloud masking matter. *Remote Sens. Environ.*, **127**, 370–384, doi:10.1016/j.rse.2012.08.035.
- Hurrell, J., J. Hack, D. Shea, J. Caron, and J. Rosinski, 2008: A new sea surface temperature and sea ice boundary dataset for the community atmosphere model. *J. Climate*, **21**, 5145–5153.
- Jackson, R. B., J. Canadell, J. R. Ehleringer, H. A. Mooney, O. E. Sala, and E. D. Schulze, 1996: A global analysis of root distributions for terrestrial biomes. *Oecologia*, **108**, 389–411.
- Jipp, P. H., D. C. Nepstad, D. K. Cassel, and C. R. De Carvalho, 1998: Deep soil moisture storage and transpiration in forests and pastures of seasonally-dry Amazonia. *Climatic Change*, **39**, 395–412.
- Kalnay, E., and Coauthors, 1996: The NCEP/NCAR 40-Year Reanalysis Project. *Bull. Amer. Meteor. Soc.*, **77**, 437–471.
- Lathuilliere, M. J., M. S. Johnson, and S. D. Donner, 2012: Water use by terrestrial ecosystems: Temporal variability in rainforest and agricultural contributions to evapotranspiration in Mato Grosso, Brazil. *Environ. Res. Lett.*, **7**, 024024, doi:10.1088/1748-9326/7/2/024024.
- Lee, J. E., R. S. Oliveira, T. E. Dawson, and I. Fung, 2005: Root functioning modifies seasonal climate. *Proc. Natl. Acad. Sci. USA*, **102**, 17 576–17 581.
- , B. R. Lintner, C. K. Boyce, and P. J. Lawrence, 2011: Land use change exacerbates tropical South American drought by sea surface temperature variability. *Geophys. Res. Lett.*, **38**, L19706, doi:10.1029/2011GL049066.



- Lewis, S. L., P. M. Brando, O. L. Phillips, G. M. F. van der Heijden, and D. Nepstad, 2011: The 2010 Amazon drought. *Science*, **331**, 554.
- Li, W. H., and R. Fu, 2004: Transition of the large-scale atmospheric and land surface conditions from the dry to the wet season over Amazonia as diagnosed by the ECMWF reanalysis. *J. Climate*, **17**, 2637–2651.
- Liebmann, B., and J. A. Marengo, 2001: Interannual variability of the rainy season and rainfall in the Brazilian Amazon basin. *J. Climate*, **14**, 4308–4318.
- Lin, X., D. A. Randall, and L. D. Fowler, 2000: Diurnal variability of the hydrologic cycle and radiative fluxes: Comparisons between observations and a GCM. *J. Climate*, **13**, 4159–4179.
- Los, S. O., and Coauthors, 2000: A global 9-yr biophysical land surface dataset from NOAA AVHRR data. *J. Hydrometeorol.*, **1**, 183–199.
- Malhado, A., M. H. Costa, F. Z. de Lima, K. C. Portilho, and D. N. Figueiredo, 2009: Seasonal leaf dynamics in an Amazonian tropical forest. *For. Ecol. Manage.*, **258**, 1161–1165.
- Malhi, Y., and J. Wright, 2004: Spatial patterns and recent trends in the climate of tropical rainforest regions. *Philos. Trans. Roy. Soc. London*, **B359**, 311–329.
- , J. T. Roberts, R. A. Betts, T. J. Killeen, W. H. Li, and C. A. Nobre, 2008: Climate change, deforestation, and the fate of the Amazon. *Science*, **319**, 169–172.
- Marengo, J. A., 2004: Interdecadal variability and trends of rainfall across the Amazon basin. *Theor. Appl. Climatol.*, **78**, 79–96.
- , 2006: On the hydrological cycle of the Amazon basin: A historical review and current state-of-the-art. *Rev. Bras. Meteorol.*, **21**, 1–19.
- , C. A. Nobre, J. Tomasella, M. F. Cardoso, and M. D. Oyama, 2008a: Hydro-climatic and ecological behaviour of the drought of Amazonia in 2005. *Philos. Trans. Roy. Soc. London*, **B363**, 1773–1778.
- , and Coauthors, 2008b: The drought of Amazonia in 2005. *J. Climate*, **21**, 495–516.
- , J. Tomasella, L. Alves, W. Soares, and D. Rodriguez, 2011: The drought of 2010 in the context of historical droughts in the Amazon region. *Geophys. Res. Lett.*, **38**, L12703, doi:10.1029/2011GL047436.
- McKee, T., N. Doesken, and J. Kleist, 1993: The relationship of drought frequency and duration to time scales. *Proc. Eighth Conf. on Applied Climatology*, Anaheim, CA, Amer. Meteor. Soc., 179–184.
- Miller, S., M. Goulden, M. Menton, H. da Rocha, H. de Freitas, A. Figueira, and C. de Sousa, 2004: Biometric and micrometeorological measurements of tropical forest carbon balance. *Ecol. Appl.*, **14** (Suppl.), S114–S126.
- Myneni, R. B., and Coauthors, 2007: Large seasonal swings in leaf area of Amazon rainforests. *Proc. Natl. Acad. Sci. USA*, **104**, 4820–4823, doi:10.1073/pnas.0611338104.
- NCL, 2013: The NCAR command language (version 6.1.1). UCAR/NCAR/CISL/VETS. [Available online at <http://www.ncl.ucar.edu/>.]
- Nepstad, D. C., and Coauthors, 1994: The role of deep roots in the hydrological and carbon cycles of Amazonian forests and pastures. *Nature*, **372**, 666–669.
- , I. M. Tohver, D. Ray, P. Moutinho, and G. Cardinot, 2007: Mortality of large trees and lianas following experimental drought in an Amazon forest. *Ecology*, **88**, 2259–2269.
- , C. Stickler, B. Soares, and F. Merry, 2008: Interactions among Amazon land use, forests and climate: Prospects for a near-term forest tipping point. *Philos. Trans. Roy. Soc. London*, **B363**, 1737–1746, doi:10.1098/rstb.2007.0036.
- Oliveira, R. S., T. E. Dawson, S. S. O. Burgess, and D. C. Nepstad, 2005: Hydraulic redistribution in three Amazonian trees. *Oecologia*, **145**, 354–363.
- Pan, D. M., and D. A. Randall, 1998: A cumulus parametrization with a prognostic closure. *Quart. J. Roy. Meteor. Soc.*, **124**, 949–981.
- Phillips, O. L., and Coauthors, 2009: Drought sensitivity of the Amazon rainforest. *Science*, **323**, 1344–1347.
- , and Coauthors, 2010: Drought-mortality relationships for tropical forests. *New Phytol.*, **187**, 631–646.
- Powell, T. L., and Coauthors, 2013: Evaluating model predictions of carbon fluxes for Amazonian rainforests subjected to severe drought. *New Phytol.*, **200**, 350–365, doi:10.1111/nph.12390.
- Randall, D. A., J. A. Abeles, and T. G. Corsetti, 1985: Seasonal simulations of the planetary boundary layer and boundary layer stratocumulus clouds with a general circulation model. *J. Atmos. Sci.*, **42**, 641–676.
- , and Coauthors, 1996: A revised land surface parameterization (SiB2) for GCMS. Part III: The greening of the Colorado State University general circulation model. *J. Climate*, **9**, 738–763.
- Ringler, T. D., R. P. Heikes, and D. A. Randall, 2000: Modeling the atmospheric general circulation using a spherical geodesic grid: A new class of dynamical cores. *Mon. Wea. Rev.*, **128**, 2471–2490.
- Ropelewski, C. F., and M. S. Halpert, 1987: Global and regional scale precipitation patterns associated with the El Niño/Southern Oscillation. *Mon. Wea. Rev.*, **115**, 1606–1626.
- Saatchi, S. S., R. A. Houghton, R. Alvala, J. V. Soares, and Y. Yu, 2007: Distribution of aboveground live biomass in the Amazon basin. *Global Change Biol.*, **13**, 816–837, doi:10.1111/j.1365-2486.2007.01323.x.
- , and Coauthors, 2011: Benchmark map of forest carbon stocks in tropical regions across three continents. *Proc. Natl. Acad. Sci. USA*, **108**, 9899–9904.
- , S. Asefi-Najafabady, Y. Malhi, L. Aragao, L. Anderson, R. Myneni, and R. Nemani, 2013: Persistent effects of a severe drought on Amazonian forest canopy. *Proc. Natl. Acad. Sci. USA*, **110**, 565–570.
- Saleska, S. R., K. Didan, A. R. Huete, and H. R. da Rocha, 2007: Amazon forests green-up during 2005 drought. *Science*, **318**, 612.
- Samanta, A., S. Ganguly, H. Hashimoto, S. Devadiga, E. Vermote, Y. Knyazikhin, R. R. Nemani, and R. B. Myneni, 2010: Amazon forests did not green-up during the 2005 drought. *Geophys. Res. Lett.*, **37**, L05401, doi:10.1029/2009GL042154.
- , —, E. Vermote, R. R. Nemani, and R. B. Myneni, 2012: Why is remote sensing of Amazon forest greenness so challenging? *Earth Interact.*, **16**, doi:10.1175/2012EI440.1.
- Sellers, P. J., Y. Mintz, Y. C. Sud, and A. Dalcher, 1986: A Simple Biosphere Model (SiB) for use within general circulation models. *J. Atmos. Sci.*, **43**, 505–531.
- , J. A. Berry, G. J. Collatz, C. B. Field, and F. G. Hall, 1992: Canopy reflectance, photosynthesis, and transpiration. III. A reanalysis using improved leaf models and a new canopy integration scheme. *Remote Sens. Environ.*, **42**, 187–216.
- , and Coauthors, 1996a: A revised land surface parameterization (SiB2) for atmospheric GCMS. Part I: Model formulation. *J. Climate*, **9**, 676–705.
- , S. O. Los, C. J. Tucker, C. O. Justice, D. A. Dazlich, G. J. Collatz, and D. A. Randall, 1996b: A revised land surface

- parameterization (SiB2) for atmospheric GCMS. Part II: The generation of global fields of terrestrial biophysical parameters from satellite data. *J. Climate*, **9**, 706–737.
- Spracklen, D. V., S. R. Arnold, and C. M. Taylor, 2012: Observations of increased tropical rainfall preceded by air passage over forests. *Nature*, **489**, 282–285.
- Stephens, G. L., P. M. Gabriel, and P. T. Partain, 2001: Parameterization of atmospheric radiative transfer. Part I: Validity of simple models. *J. Atmos. Sci.*, **58**, 3391–3409.
- Suarez, M. J., A. Arakawa, and D. A. Randall, 1983: The parameterization of the planetary boundary layer in the UCLA general circulation model: Formulation and results. *Mon. Wea. Rev.*, **111**, 2224–2243.
- Taylor, I. H., E. Burke, L. McColl, P. Falloon, G. R. Harris, and D. McNeill, 2012: Contributions to uncertainty in projections of future drought under climate change scenarios. *Hydrol. Earth Syst. Sci. Discuss.*, **9**, 12 613–12 653, doi:10.5194/hessd-9-12613-2012.
- Taylor, K., D. Williamson, and F. Zwiers, 2000: AMIP II sea surface temperature and sea ice concentration boundary conditions. PCMDI Rep. 60. [Available online at <http://www.pcmdi.llnl.gov/projects/amip/AMIP2EXPDSN/BCS/amip2bcs.php>.]
- Toomey, M., D. A. Roberts, C. Still, M. L. Goulden, and J. P. McFadden, 2011: Remotely sensed heat anomalies linked with Amazonian forest biomass declines. *Geophys. Res. Lett.*, **38**, L19704, doi:10.1029/2011gl049041.
- Trenberth, K. E., 1999: Atmospheric moisture recycling: Role of advection and local evaporation. *J. Climate*, **12**, 1368–1381.
- Tucker, C. J., J. E. Pinzon, M. E. Brown, D. A. Slayback, E. W. Pak, R. Mahoney, E. F. Vermote, and N. El Saleous, 2005: An extended AVHRR 8-km NDVI dataset compatible with MODIS and spot vegetation NDVI data. *Int. J. Remote Sens.*, **26**, 4485–4498.
- Vidale, P. L., and R. Stockli, 2005: Prognostic canopy air space solutions for land surface exchanges. *Theor. Appl. Climatol.*, **80**, 245–257.
- von Randow, R. C. S., C. von Randow, R. W. A. Hutjes, J. Tomasella, and B. Kruijt, 2012: Evapotranspiration of deforested areas in central and southwestern Amazonia. *Theor. Appl. Climatol.*, **109**, 205–220.
- Vourlitis, G., F. Lobo, P. Zeilhofer, and J. Nogueira, 2011: Temporal patterns of net CO<sub>2</sub> exchange for a tropical semi-deciduous forest of the southern Amazon basin. *J. Geophys. Res.*, **116**, G03029, doi:10.1029/2010JG001524.
- Xu, L. A., A. Samanta, M. H. Costa, S. Ganguly, R. R. Nemani, and R. B. Myneni, 2011: Widespread decline in greenness of Amazonian vegetation due to the 2010 drought. *Geophys. Res. Lett.*, **38**, L07402, doi:10.1029/2011GL046824.
- Yin, L., R. Fu, E. Shevliakova, and R. E. Dickinson, 2013: How well can CMIP5 simulate precipitation and its controlling processes over tropical South America? *Climate Dyn.*, doi:10.1007/s00382-012-1582-y, in press.
- Zeng, N., J.-H. Yoon, J. Marengo, A. Subramaniam, C. A. Nobre, A. Mariotti, and J. D. Neelin, 2008: Causes and impacts of the 2005 Amazon drought. *Environ. Res. Lett.*, **3**, 014002, doi:10.1088/1748-9326/3/1/014002.